

THE EFFECT OF SPREADING COEFFICIENT ON RECOVERY OF WATERFLOOD RESIDUAL OIL USING GAS INJECTION IN FRACTURED CARBONATE ROCKS: A MICRO-SCALE EXPERIMENTAL INVESTIGATION USING X-RAY MICROTOMOGRAPHY

M. Sabti, A.H. Alizadeh, E. Lowry, and M. Piri
Department of Petroleum Engineering, University of Wyoming,
1000 E. University Ave., Laramie, WY 82071-2000, USA

This paper was prepared for presentation at the International Symposium of the Society of Core Analysts held in Vienna, Austria, 27 August – 1 September 2017

ABSTRACT

Fractured carbonate reservoirs host a significant fraction of oil reserves around the world. Enhancing the recovery of oil from these reservoirs requires a considerably improved understanding of the displacement mechanisms governing the fluid transport from the matrix to the fracture network. During the last few decades, a considerable amount of effort has been dedicated to developing laboratory and field technologies to overcome the challenges associated with the complex flow behavior in these reservoirs during recovery processes. In this paper, we present the results of a pore-scale experimental study of tertiary gas injection in a fractured carbonate rock sample. A state-of-the-art, three-phase miniature core-flooding apparatus integrated with a high-resolution micro-CT scanner was employed to conduct two sets of three-phase brine/oil/gas experiments under spreading and nonspreading conditions. The initial two-phase, oil-water saturation conditions prior to gas injection were similar for both spreading and nonspreading fluid systems. The core sample, 10 mm in diameter and 48 mm long, was partially fractured to the middle, along the length of the specimen, in order to probe multiphase flow behavior in various topological locations of the sample including the matrix and the fracture in order to better understand matrix-fracture interactions. We developed an image processing workflow to map the pore fluid occupancies and fluid connectivity in both the fracture and the matrix. This allowed us to examine the impact of the spreading phenomena on oil extraction from the matrix to the fracture. During gas injection, since gas-liquid capillary pressures were negligible in the fracture conduit, gas displaced brine first. By increasing the gas flow rate in the spreading system, gas accessed trapped oil globules in the neighboring matrix, resulting in formation of spreading oil layers and re-connection of trapped oil globules. It was found that the ability of oil to maintain its hydraulic connectivity between the matrix and fracture by forming stable spreading layers, sandwiched between brine in the corners of pore elements and gas in their centers, improved the oil recovery efficiency significantly. Oil layer drainage, however, was not observed in the experiment performed with the nonspreading fluid system, resulting in higher remaining oil saturation.

INTRODUCTION

The infrequent discovery of new, producible oil fields has led the petroleum community to research new approaches to enhance the extraction of the remaining oil after primary or secondary recovery, particularly for complicated reservoir rock morphologies, such as fractured reservoirs. This type of reservoirs is one of the most important geological formations targeted for oil recovery by petroleum industry since they host a vast fraction of oil reserves worldwide. Further oil production from these reservoirs often requires the injection of a new fluid phase, in addition to oil and brine already present in the reservoir, to enhance the oil displacement efficiency from the matrix to the fractures. The coexistence of three fluid phases, such as brine, oil, and gas, within a fractured system introduces technical challenges in addition to the disparate hydraulic conductivity of the matrix blocks compared to the fracture network. The displacement mechanisms taking place under three-phase flow conditions, such as layer drainage, however, may play a significant role in connecting the matrix to the fracture by forming spreading oil layers and hence increasing the oil recovery. Layer drainage, in a porous medium saturated with brine, oil, and gas, refers to a process under which oil is displaced by gas in the presence of brine through stable and connected layers. Although a number of studies in the literature [1-4] have been dedicated to understanding the spreading phenomena and their impacts on remaining oil saturation, most of these investigations probed nonfractured porous media and did not consider the presence of fractures. Blunt et al. [2] discussed the importance of the spreading layers theoretically and experimentally. They performed gravity drainage experiments using sand columns and capillary tubes and concluded that the stability of oil layers in the spreading system provided hydraulic continuity for the oil phase and resulted in higher oil recovery. For the nonspreading system, however, less oil recovery was observed. Vizika and Lombard [3] investigated the effect of spreading characteristics on residual oil saturation. They carried out secondary gravity assisted inert gas injection experiments on a consolidated porous medium using fluid systems with positive and negative spreading coefficients. Under water-wet conditions, the oil relative permeability was almost identical at high oil saturations for both the spreading and nonspreading systems but showed differences at low oil saturations where layer flow played a more significant role. Zhou and Blunt [5], Sahni et al. [6], Alizadeh and Piri [7], and Øren and Pinczewski [8] also observed the impact of the flow through spreading layers experimentally. A recent study by Zolfaghari and Piri [9] investigated the formation and collapse of the spreading oil layers and oil cusps using thermodynamically consistent threshold capillary pressures and a three-phase pore-scale network model. The authors extensively investigated the effect of layer and cusp stability on three-phase relative permeabilities and validated their predictions against core-scale results reported by Alizadeh and Piri [7] and others in the literature.

Despite the knowledge gained through the above-mentioned studies on non-fractured systems, laboratory and field studies can be further expanded to improve our understanding about the fundamentals of multi-phase flow in fractured porous media. Over the last few years, researchers and scientists have been motivated to use the so-called “digital rock physics” workflow, which includes the interpretation of rock properties and in-situ fluid occupancies using advanced imaging technologies, such as X-ray microtomography [10].

This approach provides a mean for direct observation of pore space topology and fluid occupancy on a wide range of scales from millimeters to nanometers. This methodology allows researchers to verify previously-hypothesized multi-phase flow displacement theories.

In this study, a state-of-the-art experimental system including a high-resolution micro-CT scanner integrated with a three-phase core-flooding apparatus was utilized to perform two- and three-phase flow experiments on a miniature fractured carbonate core sample. The study was designed to demonstrate the role of spreading phenomena in displacing oil from the matrix to the fracture at the pore scale. The pore fluid occupancies were compared under spreading and nonspreading conditions during gas injection experiments.

MATERIALS AND METHODS

Rock sample and fluids

Fond Du Lac limestone quarried from an outcrop area in Wisconsin, USA, was selected for this study. It is a water-wet rock consisting mainly of calcium carbonate. A core plug, 38 mm in diameter and 120 mm long, was cut from a block of the selected rock using water and then oven dried at 110° C for 24 hours. Subsequently, a fracture was introduced into half of the core plug, i.e., from one of the end faces to nearly the middle of the medium as shown in Figure 1 (a, b). The fracture was induced by applying a non-uniform stress parallel to the stress axis of the core plug using the modified Brazilian test [11, 12]. The core plug was then X-ray imaged using a medical CT scanner to visualize the fracture and its orientation throughout the pore space. A miniature core samples, 10 mm in diameter and 48 mm in length, was cut from the fractured core plug using air as a coolant. The miniature sample was drilled in a way that the fracture was positioned in the middle of its cross section as illustrated in Figure 1 (b, c). The end faces of the miniature core sample were trimmed so that the fracture extended only over half of sample's length. The dimensions and the petrophysical properties of the miniature core sample are given in Table 1.

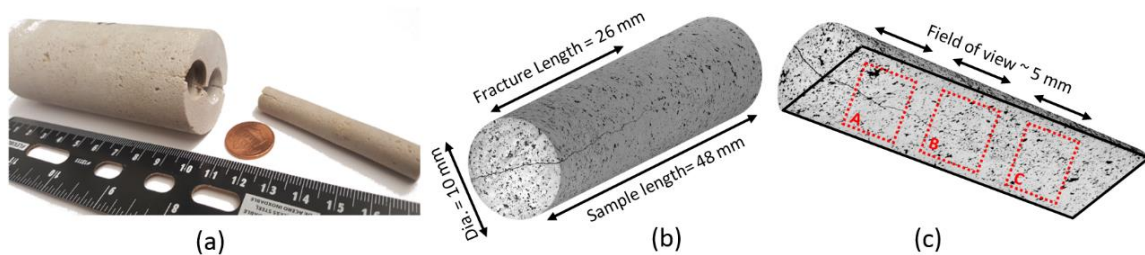


Figure 1. (a) The miniature sample drilled from the core plug, (b) a three-dimensional representation of the miniature sample, and (c) scan locations (i.e., A, B, and C) and their fields of view.

The core-flooding tests were carried out using two fluid systems with different spreading coefficients. The only difference between the two fluid systems was the oil phases used. The aqueous phase (i.e., the wetting phase) was prepared using distilled water, 2 wt% CaCl₂, 15 wt% NaI as an X-ray doping agent, and 0.01 wt% NaN₃ as an anti-bacterial

growth agent. A sacrificial limestone core was immersed in the aqueous solution for 24 hours in order to equilibrate the brine with the rock minerals and prevent rock dissolution during injection sequences. The oil phases (i.e., the intermediate-wetting phase) were Soltrol 170 for the spreading system and White Mineral Oil for the nonspreading system. Both oils were well purified prior to use by passing them through a gravity column filled with aluminum oxide (alumina) and silica gel to remove polar components and surface active impurities that could alter the wettability of the medium. In both fluid systems, 5 vol% 1-iodooctane ($C_8H_{17}I$) was added to the oils as an X-ray dopant. Sodium iodide and 1-iodooctane were used to establish sufficient contrasts among the fluid phases. The gaseous phase (i.e., the most nonwetting phase) was nitrogen with 99.9% purity. Table 2 lists the properties of the fluids used.

Table 1: Dimensions and petrophysical properties of the miniature core sample used in the experiments.

Rock	Length (mm)	Diameter (mm)	Porosity of the matrix (%) [*]	Gas permeability of the matrix (mD) [*]	Pore volume (ml)
Fond Du Lac limestone	47.98	9.98	10.9	13.8	0.4

^{*}Porosity and permeability were measured on the core plug before creating the fracture using an automated helium porosimeter-permeameter.

Table 2: Properties of the fluids used in this study.

Fluid	Viscosity (mPa.s)	Density (kg/m ³)
Brine (2 wt% CaCl ₂ + 15 wt% NaI + 0.01 wt% NaN ₃)	1.145	1138.12
Spreading oil (Soltrol 170)	2.526	802.13
Nonspreading oil (white mineral oil)	26.367	805.02
Gas (Nitrogen)	0.0187	62.84

Experimental apparatus

The experimental apparatus used in this work consisted of a three-phase core-flooding setup coupled with a high-resolution micro CT scanner (Xradia 510 Versa). As shown in Figure 2, the core-flooding setup included a miniature core holder, Rosemount[®] differential pressure transducers with different ranges, a three-phase separator, two accumulators, and six dual-cylinder Quizix[®] pumps. Three of the pumps were utilized to inject brine, oil, and gas into the core, one pump to maintain overburden pressure, one pump to receive the fluids produced from the core and regulate the pore pressure, and the last pump to compensate for fluctuations in the separator pressure caused by fluid withdrawal/accumulation. The wetted parts were made of Hastelloy C-276 to prevent corrosion. Inside the micro-CT enclosure, the core holder was connected to high pressure PEEK (polyetheretherketon) tubing. This tubing is light-weight and flexible so it minimizes the amount of torque exerted on the core-holder during the rotation, which could severely impact the quality of images. An in-house custom-designed core holder was fabricated from carbon fiber because it is fully X-ray transparent and lightweight as well as having a high strength-to-weight ratio. It helps to significantly reduce scanning time and noise. The design of the core-flooding setup allowed for the equilibration of the three fluids (water/oil/gas) in a closed-loop bypassing the core prior to starting the experiment to avoid any mass transfer between the

phases. This system also allowed to dynamically scan the medium while injecting the fluids into the core sample. This feature enabled us to compare the pore fluid occupancies at exactly the same locations in the core sample during the course of the experiments without altering the pore configurations and fracture aperture. More details of the three-phase core-flooding setup can be found elsewhere [13].

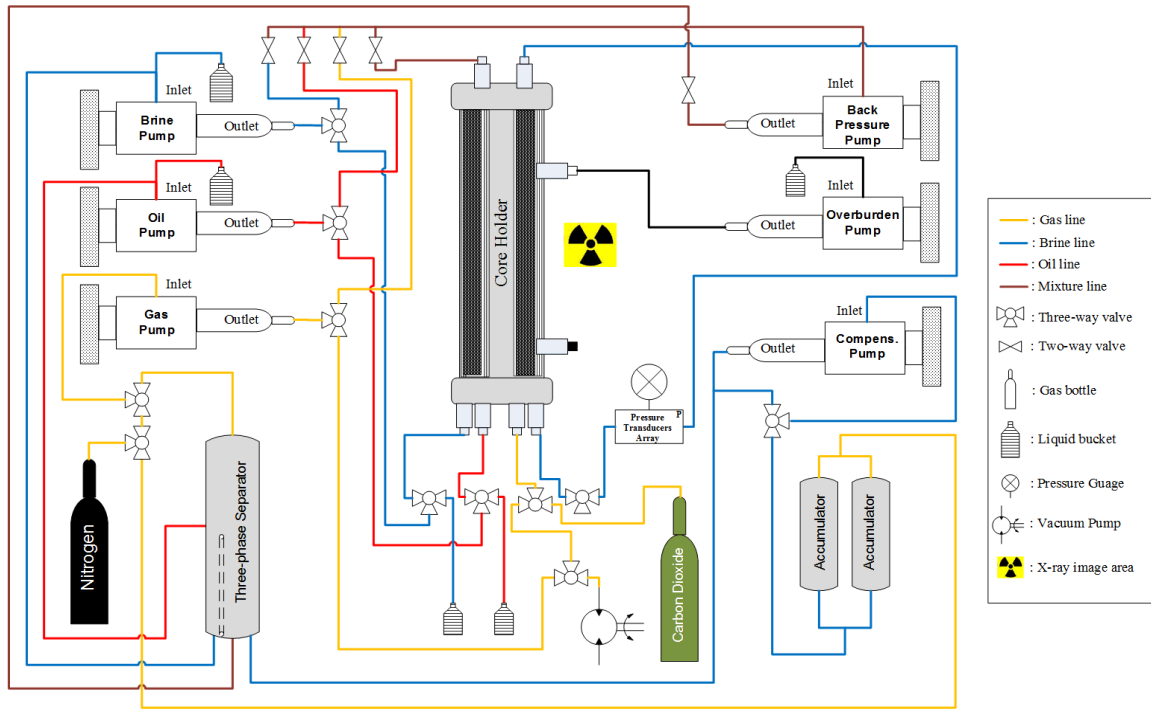


Figure 2. Experimental setup employed to perform the core-flooding experiments. The core holder was placed inside the micro-CT scanner's enclosure [14].

Experimental procedure

The core holder was placed vertically inside the micro-CT scanner, and then an overburden pressure of 100 psig was applied on the core sample. The fractured end face of the sample was placed at the bottom where the phases were injected from. After acquiring a reference scan with a resolution of $2.5 \mu\text{m}$, the sample was flooded with gaseous CO_2 , vacuumed, and subsequently fully saturated with degassed brine. The pore and overburden pressures were then concurrently increased to 500 and 600 psig, respectively, and several pore volumes of brine were injected into the sample. The net confining pressure of 100 psi was maintained in the course of all displacements to avoid any undesirable changes in the aperture of the fracture. After saturating the medium with brine, the core sample was scanned again to acquire a new reference image. Subsequently, it was subjected to an oilflood to establish initial water saturation (approximately 24%) followed by a waterflood to reach residual oil saturation. Upon establishment of the initial two-phase oil-brine saturation condition, gas was injected into the sample at increasing flow rates. During all steps of the oilflood, waterflood, and gas injection processes, the core sample was regularly

scanned with a low resolution of 5 μm to monitor fluid saturations. A high-resolution scan with a resolution of 2.5 μm was taken at the end of each step when saturations no longer changed. Table 3 lists the microtomography parameters used in each type of scan. It was intended to study the pore-scale displacement physics in three different locations of the sample labeled as *A*, *B*, and *C* in Figure 1 (c). These sites were selected to study fluid displacements and pore fluid occupancies at topologically different areas of the medium while using different fluid systems. All the displacements in the experiments were conducted at 20° C and under the capillary-dominated regime. The unsteady-state approach was used to perform the experiments, in which only one phase was injected in each displacement sequence. Furthermore, the core sample was cleaned thoroughly with isopropyl alcohol between the spreading and nonspreading experiments in an attempt to use the same specimen under both conditions. Details of the cleaning process can be found elsewhere [15].

Table 3: Microtomography parameters used to scan the core sample during the core-flooding experiments.

Recipe	Projections counts	Exposure time (s)	Camera binning	Resolution (μm)	Image size (pixel)	Objective
High-resolution scan	3201	6.5	1	2.5	2032 x 2032	4.0 X
Low-resolution scan	1601	2.0	2	5	1014 x 1014	4.0 X

RESULTS AND DISCUSSION

In this section, we present the results of the two sets of experiments performed using the spreading and nonspreading fluid systems. In both sets, similar waterflood residual oil saturation conditions were established prior to gas injection. Gas was then injected into the core sample in each case and possible reduction in residual oil saturation was monitored. The subtle governing displacement mechanisms responsible for the reduction of oil saturations in both systems are highlighted.

Two-phase flow condition

The initial two-phase oil-brine condition prior to gas injection in each experiment was established by injecting oil into a fully brine saturated sample to reach an average initial brine saturation (S_{wi}) of approximately 24%. This was followed by a waterflood to establish residual oil saturation (S_{orw}). The waterflood residual oil saturations obtained in the spreading and nonspreading experiments were 52 and 47%, respectively. We attempted to reach similar initial two-phase oil-brine saturation conditions in both spreading and nonspreading experiments to examine the impact of the spreadability of the oil on recovery of waterflood residual oil during gas injection. Since the oil viscosities in this study were different by an order of magnitude (see Table 2), a modified capillary number equation, $N_{ca} = \frac{\mu_w v_w}{\gamma_{ow} \phi} \left(\frac{\mu_w}{\mu_o}\right)^{0.4}$ [16], that accounts for the viscosity of the defending fluid (i.e., oil), was used to determine the waterflooding flow rate preceding the gas injection tests. In this equation, μ is viscosity, ϕ is porosity, γ is interfacial tension between the pairs of fluids, and v is Darcy velocity. The subscripts w and o denote brine and oil, respectively.

By analyzing the images, it was observed that oil, the nonwetting phase with respect to brine, initially filled the fracture as it constituted the path of the least resistance. As primary oil drainage progressed and the capillary pressure increased, oil started to invade the large brine-filled pore elements in the neighboring matrix. Brine, as the wetting-phase, covered the surface and the roughness of the pore and fracture walls and formed wetting layers in the corners of the pores. Figures 3(a) to (c) show the pore fluid occupancy of brine and oil starting from a dry void space to an initial brine saturation condition in an intra-fracture spacing. The brine was connected through the wetting layers that covered the solid surface throughout the medium. During the waterflood, which was conducted under the capillary dominated flow regime ($N_{ca} \sim 10^{-6}$), brine initially invaded small pore elements of the matrix as well as the narrow parts of the fracture aperture. By increasing the brine flow rate, local oil-water capillary pressure decreased allowing water to invade into larger elements and wider openings of the fracture as well. As expected, the imbibition threshold capillary pressures regulated the displacement sequence. As brine flow rate was increased to higher values, the brine layers swelled in many of the pore elements that in turn led trapped oil in the matrix and the narrow openings of the fracture by the snap-off displacement mechanism. This can be seen in Figure 3(d) where trapping of an oil globule in a selected fracture opening is illustrated.

Three-phase flow condition

Upon establishment of the waterflood residual oil, gas (the most nonwetting phase) was injected into the core sample. When gas is introduced to a water-wet porous medium having oil and brine, various possible displacement scenarios may result in the drainage of oil and brine: (1) gas displaces oil (gas-to-oil), (2) gas displaces brine (gas-to-brine), (3) gas displaces oil and oil displaces brine (gas-to-oil-to-brine), and (4) gas displaces brine and brine displaces oil (gas-to-brine-to-oil) [17]. The occurrence of these scenarios depends on many factors including the pore occupancy established before gas injection.

The analysis of the micro-CT images revealed that the injected gas initially propagated the fracture conduit due to the minimal gas-water threshold capillary pressure required. At very low gas flow rates, gas did not virtually invade the pore elements of the matrix adjoining the fracture and no oil displacement was observed in the surrounding matrix. By increasing the gas flow rate, the gas-brine capillary pressure overcame its displacement threshold values and gas invaded the matrix. At this juncture, the gas displaced brine first since brine was mobile and then reached the trapped oil blobs. After reaching these blobs, gas started to displace oil. The displaced oil could in turn displace brine, resulting in a double displacement event. This gas-to-oil-to-brine event was observed to be more favorable and frequent than gas-to-brine-to-oil. This finding has also been reported in previous studies [4,8,18]. The scenario during which gas displaces oil but oil does not displace brine was not observed in this study because the oil was initially trapped. This displacement event, however, was observed in our previous studies under secondary gas injection into a fractured porous medium where the wetting phase, brine, was immobile [15,19]. One should note that the spreadability of oil will also impact the oil displacement, which is explained in the next section.

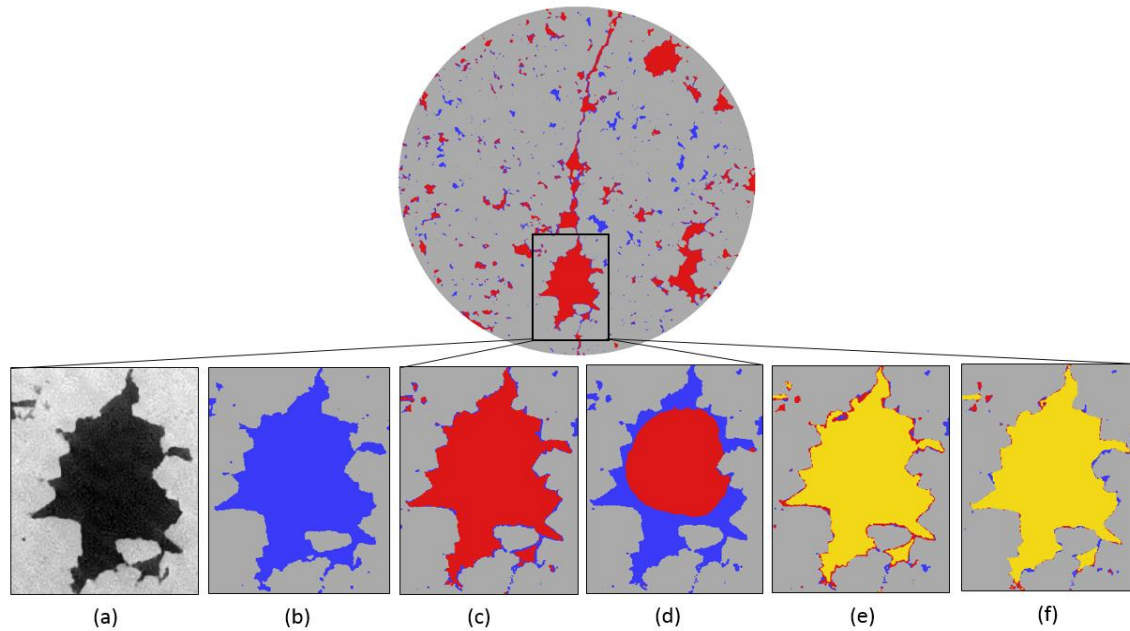


Figure 3. Segmented images showing the fluid occupancy map of an intra-fracture spacing at Location A during gas injection; (a) gray-scale image of the void space, (b) after fully saturation with brine, (c) after primary oil drainage, (d) after the waterflood, (e) after gas injection (in the spreading system), and (f) after gas injection (in the nonspreading system). Black, blue, red, yellow, and gray represent the void space, brine, oil, gas, and grains, respectively. The images were taken with a resolution of $2.5 \mu\text{m}$ and a field of view of 5 mm.

Spreading and nonspreading systems

The ability of oil to spread on water in the presence of gas is characterized by the oil spreading coefficient. It is defined as $S = \gamma_{gw} - (\gamma_{go} + \gamma_{ow})$, where γ_{gw} , γ_{go} , and γ_{ow} are the interfacial tension of gas-water, gas-oil, and oil-water pairs, respectively. When water, oil, and gas coexist in a system at equilibrium, the spreading coefficient can be either zero or negative. A zero or slightly negative value implies that oil will spread as a thin layer between water and gas with a non-negligible hydraulic conductivity. In contrast, a negative value means that oil will form a disconnected lens on the surface of water in the presence of gas and, hence, will not sustain its phase connectivity across the medium. The thickness and the stability of these layers depend on the spreading coefficient, pore geometry, and gas flow rate [7,8,9,20].

In the spreading experiment, as gas flow rate was increased (resulting in increasing the gas-water capillary pressure), gas reached the trapped oil globules. At this point, oil started forming continuous and stable spreading oil layers between brine and gas, which allowed oil to get reconnected. Subsequently, gas started to drain oil through these layers from the matrix to the fracture and towards production site. Figure 4 illustrates the tendency of oil to spread on the surface of water in the presence of gas. In this figure, a gas cluster invaded

a pore element that held trapped oil in the center and brine in the corners. As shown, oil spread and evolved into oil layer between the gas cluster and the brine. The analysis of the CT images of the spreading experiment further confirms that the spreading characteristics aided in maintaining oil-phase connectivity from the matrix to the fracture and hence enhanced the oil production (Figure 5). As seen in this figure, the oil formed a continuous layer that spread between the brine and gas and allowed for hydraulic connectivity of the oil in both the fracture and the matrix. However, in the nonspreading experiment, as the gas flow rate was increased, the oil globules did not possess the tendency to form spreading layers, thereby limiting the amount of oil that could be drained from the matrix to the fracture.

The ternary diagrams depicted in Figure 6 show the saturation paths for both the spreading and nonspreading oil experiments in both the neighboring matrix of the fractured portion of the core as well as the matrix-only site. In both locations, it can be seen that the gas initially displaced a large amount of brine at a relatively low flow rate of gas and then displaced more oil in the spreading system. However in the nonspreading system, the oil and the brine were displaced simultaneously with lower efficiency due to the characteristics of this system and the larger pressure required to displace the highly viscous disconnected trapped oil phase. This is evident by comparing the reduction of oil saturation in both spreading and nonspreading systems in Figure 6. As a result of the differences in the displacement mechanisms between the spreading and nonspreading systems, the saturation of oil at the end of gas injection reached as low as 14% for the spreading system compared to 27% in the nonspreading system.

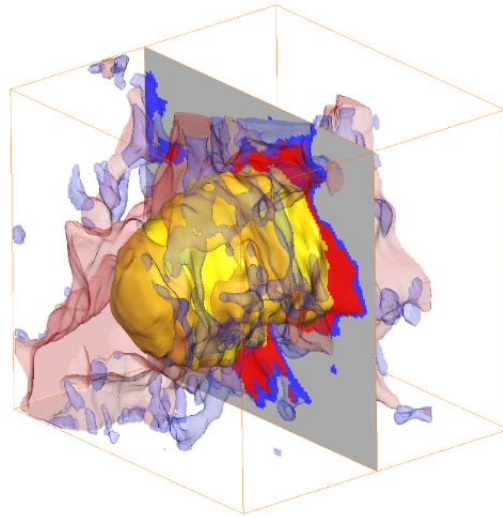


Figure 4. Segmented image showing the fluid occupancy map obtained during gas injection with a resolution of 2.5 μm . Faded blue/blue, faded red/red, yellow, and gray colors represent brine, oil, gas, and grains, respectively.

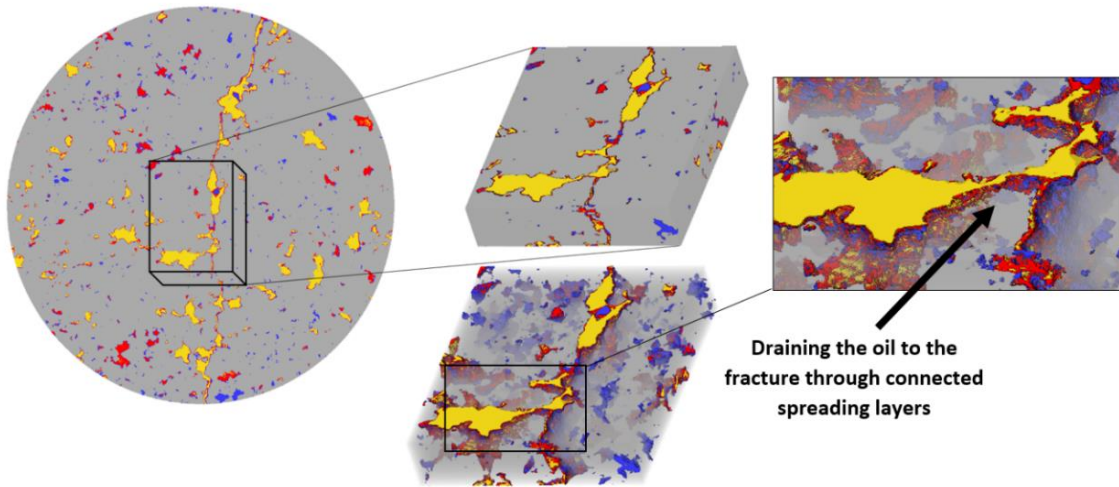


Figure 5. Segmented images showing the fluid occupancy during gas injection. Oil was drained from a pore element to the fracture through spreading layers. Faded blue/blue, faded red/red, yellow, and gray colors represent brine, oil, gas, and grains, respectively. The images were taken with a resolution of 2.5 μm .

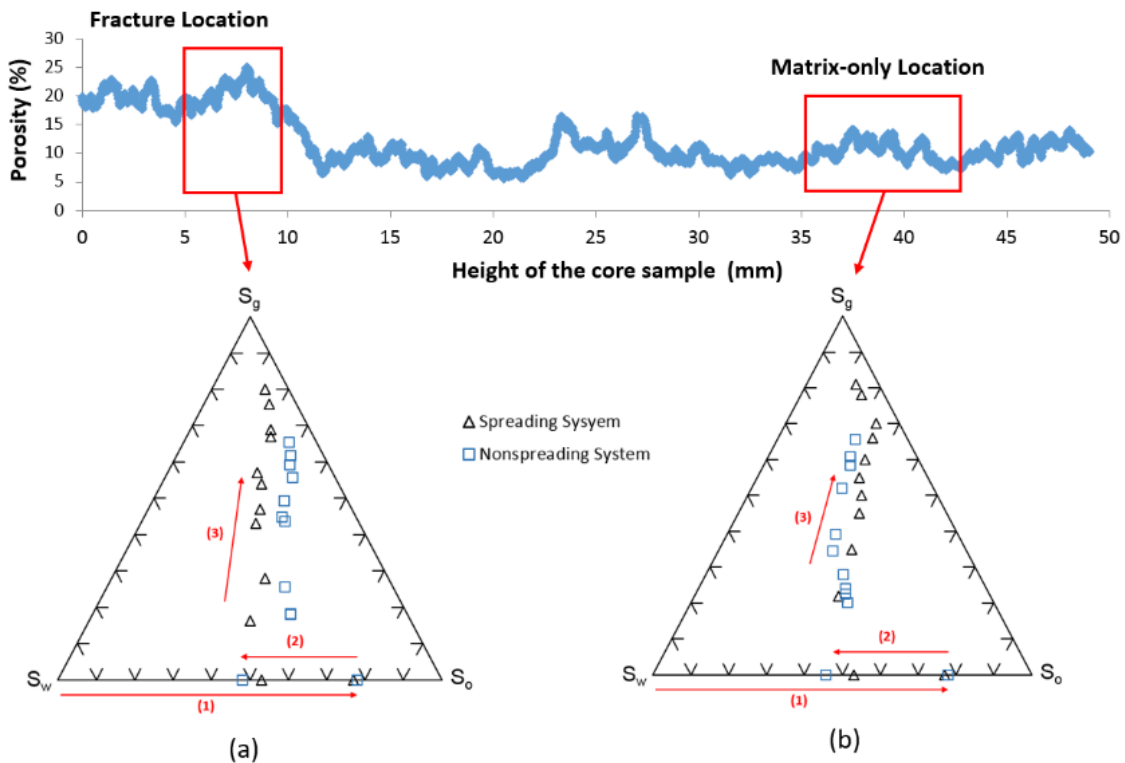


Figure 6. Saturation trajectories taken during the flow tests under spreading and nonspreading systems. The points represent fluid saturations measured (a) at Location A (matrix surrounding the fracture) and (b) at Location C (only matrix). (1), (2) and (3) represent oil drainage, waterflood and gas injection displacement sequences, respectively.

CONCLUSION

The formation of spreading layers strongly enhanced the hydraulic conductivity of the reconnected trapped oil from the matrix to the fracture, which resulted in much higher ultimate oil recovery as compared to the nonspreading system. This was confirmed by capturing a detailed map of the pore space and fluid distributions in the intact matrix and the matrix adjacent to the fracture under two- and three-phase flow conditions using X-ray micro-computed tomography. These pore-scale maps demonstrated the importance of the spreading phenomena to fluid displacements under three-phase flow conditions in a fractured porous system. The saturation profile over the course of gas injection (Figure 6) showed that brine was predominately produced first since it was the most well-connected phase. The nonspreading system showed lower initial displacement of oil and brine due to the higher gas pressure required to displace the highly viscous, trapped nonspreading oil. After increasing the gas flow rate, the gas obtained sufficient capillary pressure to invade areas containing trapped oil at which point oil layers began to form and re-connect the oil phase in the spreading system. In the nonspreading system, however, these layers were not clearly observed. This study demonstrates that recovery from fractured reservoirs can be vastly improved by directly leveraging the spreading characteristics of the fluids in fractured reservoirs under tertiary gas injection.

ACKNOWLEDGEMENTS

The authors gratefully appreciate the financial support of Saudi Aramco, Hess Corporation, Kuwait Oil Company, and the School of Energy Resources at the University of Wyoming.

REFERENCES

1. Vizika, O., "Effect of the spreading coefficient on the efficiency of oil recovery with gravity drainage," proceedings of the Symposium on Enhanced Oil Recovery (1993) Denver, Colorado USA.
2. Blunt, M., D. Zhou, and D. Fenwick, "Three-phase flow and gravity drainage in porous media," *Transport in Porous Media*, (1995) **20**, 77-103.
3. Vizika, O., and J. Lombard, "Wettability and spreading: Two key parameters in oil recovery with three-phase gravity drainage," *SPE Reservoir Engineering*, (1996) **11**, 1, 54-60.
4. Keller, A., M. Blunt, and P. Roberts, "Micromodel observation of the role of oil layers in three-phase flow," *Transport in Porous Media* (1997) **26**, 277-297.
5. Zhou, D., and M., Blunt, "Effect of spreading coefficient on the distribution of light non-aqueous phase liquid in the subsurface," *Journal of Contaminant Hydrology*, (1997), **25**, 1-2.
6. Sahni, A., J. Burger, and M. Blunt, "Measurement of three phase relative permeability during gravity drainage using CT scanning," paper SPE 39655, proceeding of SPE/DOE Improved oil recovery Symposium (1998), Tulsa, Oklahoma, USA.

7. Alizadeh, A.H., and M. Piri, "The effect of saturation history on three-phase relative permeability: An experimental study," *Water Resources Research*, (2014) **50**, 1636-1664.
8. Øren, P., and W. Pinczewski, "The effect of wettability and spreading coefficients on the recovery of waterflood residual oil by miscible gasflooding," *SPE formation evaluation*, (1994) **9**, 2,149-156.
9. Zolfaghari, A., and M. Piri, "Pore-scale network modelling of three-phase flow based on thermodynamically consistent threshold capillary pressure: I: Cusp formation and collapse," *Transport in porous media*, (2017) **116**, 1093-1137.
10. Andrä, H., N. Combaret, J. Dvorkin, E. Glatt, J. Han, M. Kabel, Y. Keehm, F. Krzikalla, M. Lee, and C. Madonna, "Digital rock physics benchmarks—Part I: Imaging and segmentation", *Computer & Geosciences*, (2013) **50**, 25–32.
11. Guo, H., N.I. Aziz, and L.C. Schmidt, "Rock fracture-toughness determination by the Brazilian test," *Engineering Geology*, (1993) **33** (3), pp.177-188.
12. Alajmi, A., and A. Grader, "Analysis of Fracture-Matrix Fluid Flow Interactions Using X-ray CT," SPE 65628, Proceedings of the SPE Eastern Regional Meeting, Morgantown, West Virginia, 2000.
13. Alizadeh, A.H., M.A. Ioannidis, and M. Piri, "CO₂-saturated brine flooding: An effective process for mobilization and recovery of waterflood residual oil," paper SCA2011-07, proceeding of the Symposium of the Society of Core Analysts, (2011), Austin, Texas, USA.
14. Piri, M., Recirculating. Constant back pressure core-flooding apparatus and method., *Patent W02012/082797* (University of Wyoming, 2012).
15. Sabti, M., A.H. Alizadeh, and M. Piri, "Three-phase flow in fractured porous media: experimental investigation of matrix-fracture interactions," paper SPE 181891, presented at the SPE Annual Technical Conference, (2016), Dubai, UAE.
16. Abrams, A., "The influence of fluid viscosity, interfacial tension, and flow velocity on residual oil saturation left by waterflood," *Society of Petroleum Engineers*, (1974) **15**, (05).
17. Kantzas, A., I. Chatzis and F. Dullien, "Enhanced oil recovery by inert gas injection," paper SPE 17379, presented at SPE Enhanced Oil Recovery Symposium (1988).
18. Khishvand, M., A.H. Alizadeh, and M. Piri, "In-situ characterization of wettability and pore-scale displacement during two- and three-phase flow in natural porous media," *Advances in Water resources*, (2016) **97**, 279-298.
19. Sabti, M., A.H. Alizadeh, and M. Piri, "Matrix-fracture interactions during gas injection: A pore-scale experimental study," paper SCA2016-029, proceeding of the Symposium of the Society of Core Analysts, (2016), Snowmass, Colorado, USA.
20. Piri, M., and M. Blunt, "Three-phase threshold capillary pressures in noncircular capillary tubes with different wettabilities including contact angle hysteresis," *Physical Review E*, (2004) **70**, 061603.